



Lagrangian Oil Spill Simulation in Peter the Great Bay (Sea of Japan) with a High-Resolution ROMS Model

SERGEY V. PRANTS,¹ MAXIM V. BUDYANSKY,¹ PAVEL A. FAYMAN,¹ MICHAEL YU. ULEYSKY,¹
and ALEKSANDR A. DIDOV¹

Abstract—Oil spill incidents with tankers, port terminals and offshore platforms impact seriously on marine life and socio-economic services. They occur more and more frequently and require immediate and effective response which starts with good knowledge of the likely pathways of spilled oil in the region where a pollution has occurred. The drift of a hypothetical oil spill from the main oil port in Peter the Great Bay (PGB) in the Sea of Japan is simulated from a Lagrangian point of view based on the retrospective velocity field of the ROMS circulation model with horizontal resolution of 600 m. The particle-tracking experiments with the effects of oil evaporation and biodegradation have been performed releasing hourly passive tracers at the beginning of every month during a few years. These numerical experiments showed pathways of spilled oil in different seasons, size of the open-sea area covered by the oil and risks of coastline contamination. Three main scenarios of propagation of the spilled oil in the surface layer have been found and analyzed. In the first one, the spilled oil drifts fast away from the coast due to prevailing north/northwest winds in the cold season (from December to April). The second scenario predominantly occurs in the warm season (from May to November) with prevailing south/southeast winds when the oil slick remains near the coast in the first days after an incident. The third scenario is an intermediate one with the dispersal of the spilled oil away from the coast but not too far from the oil spill site. To explain this behavior, we used the Lyapunov maps which allowed us to identify Lagrangian fronts in the study area that shape passive tracer evolution. As a Lagrangian front moves, the oil slick moves with it. At the same time, the front acts as a transport barrier preventing cross-frontal spreading of oil.

Keywords: ROMS, sea of Japan, oil spill, Lagrangian approach, short-term prediction.

Supplementary Information The online version contains supplementary material available at <https://doi.org/10.1007/s00024-022-03197-4>.

¹ Laboratory of Nonlinear Dynamics, V.I. Il'ichev Pacific Oceanological Institute of the Far-Eastern Branch of the Russian Academy of Sciences, 43, Baltiyskaya, Vladivostok 690041, Russia. E-mail: prants@poi.dvo.ru; plaztic@poi.dvo.ru; fayman@poi.dvo.ru; uleysky@poi.dvo.ru; didov.aa@poi.dvo.ru

1. Introduction

Oil spill incidents with tankers, port terminals and offshore platforms are one of the serious problems that affect the coastal and oceanic ecosystems, natural heritage sites, commercial fisheries, marine aquaculture, and tourism. Statistics provided by the International Tanker Owners Pollution Federation (www.itopf.com/knowledge-resources/data-statistics/statistics) indicates that oil spill events continuously reported in different regions through the world. Such events occur more and more frequently Michel and Fingas (2016) and require immediate and effective response which starts with good knowledge of the likely oil pathways in the region where the pollution occurred. Reliable information on surface currents comes from high-resolution regional or global circulation models and satellite altimetry. The altimetry-based velocity field near coast is known to be not reliable Abdalla and Kolahchi (2021), and numerical models with data assimilation may be a preferable option. The model-based simulation data on oil dispersion should be incorporated into a system for monitoring, simulating, and forecasting oil spills.

In order to simulate dispersal pathways of any passively advected tracer, Lagrangian methods are especially useful. They include particle-tracking numerical experiments Varlamov et al. (1999); Varlamov and Yoon (2003); Ohshima and Simizu (2008); Ono and Ohshima (2013); Qiao and Wang (2019); Korotenko et al. (2003, 2004) with the direct integration of the velocity field and the methods based on the Lagrangian-indicator technique Prants (2014); Prants et al. (2017) which allow to track frontal structures, known as Lagrangian fronts Prants

et al. (2014a), controlling trajectories of passive tracers. As the Lagrangian front moves, the nearby tracers move along its pathway Fifani and Baudena (2021); Prants (2022). At the same time, it acts as a transport barrier preventing the cross-frontal transport of tracers Boffetta et al. (2001). Both these properties of Lagrangian fronts are very important in operational forecasting dispersion of oil spills.

A catastrophic oil spill incident occurred in the Sea of Japan with the tanker “Nakhodka” in January 1997. Cold weather conditions acted to form a very stable, persistent water-in-oil emulsion. The spilled oil traveled to unusually great distances, affected thousands of kilometers of Japan’s coastline and caused huge social and economic damage. An oil spill simulation model has been developed by Varlamov et al. (1999). This model, incorporating wind drift, random diffusion, parametrization of oil evaporation, biodegradation, and beaching, was based on a particle-tracking method using an ocean circulation model. Furthermore, an operational simulation model has also been developed Varlamov and Yoon (2003). These studies showed that ocean currents at depths of 0–15 m play the most important role in the dispersion of oil and that the reproduction of the current field is the most important for oil spill simulation.

A coupled flow/transport model has been developed to simulate a continuous oil release from the ports of the Black Sea and from the Volga River into the coastal waters of the north part of the Caspian Sea. Using predetermined model currents and Lagrangian tracking, the authors Korotenko et al. (2003), Korotenko et al. (2004) predicted the motion of individual particles, the sum of which constituted a hypothetical oil spill.

The particle-tracking numerical experiments have been conducted also for the Sea of Okhotsk near the eastern Sakhalin coast, the area of offshore oil and gas exploration and production facilities, where a high risk of incidents exists Ohshima and Simizu (2008). Similar experiments have been carried out to simulate the fate and behavior of the oil spill during January–February 2018 from the tanker “Sanchi” in the East China Sea Qiao and Wang (2019); Pan and Yu (2020). This accident led to the worst tanker spill in the last 40 years. The simulation of the oil slick trajectories for the most-likely oil spill scenarios has

been carried out in the framework of a decision support system proposed for passive and active response planning in Persian Gulf, before and after a spill Amir-Heidari and Raie (2019).

The methods, using Lagrangian coherent structures Olascoaga and Haller (2012); Duran et al. (2018), have been applied in modeling the real incidents such as the Deep Water Horizon oil spill, which occurred in the Gulf of Mexico in April 2010, the largest marine oil spill in the history of the petroleum industry. A new Lagrangian quantifier for forward time uncertainty for trajectories that are solutions of models generated from data sets has been proposed to deal with the much less catastrophic pollution event after the collision of the passenger ferry “Volcán de Tamasite” with the Nelson Mandela dike in La Luz Port in the Mediterranean Sea in April 2017 García-Sánchez et al. (2022). Lagrangian-front technique Fifani and Baudena (2021) has been applied to study the East China Sea oil spill in 2018 and the near-coast East Mediterranean incident in 2021. These methods focus on revealing geometric structures in chaotic oceanic flows which control the dispersion of a contaminated water volume in dependence on the spatial scale of spill, its location and a temporal window when it occurred.

Oil spill simulation is a complex task, as the fate and transport of the oil spill depend on several factors. The dispersal of oil at the surface and in a subsurface layer is controlled by sea currents, the wind and waves. In addition, the spilled oil also undergoes biodegradation, evaporation, emulsification and other processes, which act simultaneously and change the physicochemical properties of oil in time. The Lagrangian particle-tracking method has been widely used in recent years. In terms of the method, spilled oil is discretized into a large amount of small oil particles Varlamov et al. (1999); Varlamov and Yoon (2003); Ohshima and Simizu (2008); Ono and Ohshima (2013); Qiao and Wang (2019); MacFadyen et al. (2011); Ciappa and Costabile (2014). The spreading and entrainment of oil are not directly dependent on oil composition and tend to be linked through macro characteristics such as viscosity and density Pan and Yu (2020).

We consider spilled oil as a large number of small passive oil particles which are advected by the ocean

currents, wind and horizontal mixing. One of our tasks is to determine the potential pathways of virtual oil particles after a hypothetical spill from the Kozmino oil terminal as the first try. Computation of oil trajectories utilizes currents from the ROMS model over a comparatively short period of time, during 4–6 days after a hypothetical spill allowing us to compute particle's trajectories and Lagrangian indicators and maps. That requires a high volume of gridded wind and sea current data. We simplify the problem and consider only biodegradation and evaporation processes among different weathering processes Keramea et al. (2021). These processes have the effect of removing part of the oil from the active components of the spill.

In this paper, we simulate consequences of a hypothetical oil spill from the Kozmino crude oil terminal located in a small bay of PGB near Vladivostok city. Kozmino is the terminal point of the Eastern Siberia—Pacific Ocean pipeline and is the third-most important oil outlet in Russia (see Fig. 1). Kozmino port is meant for oil receiving through the pipeline and its transshipment to modern tankers. Port is ice-free throughout the year.

We will use the numerical circulation model (ROMS) with the horizontal resolution of 600 m and perform particle-tracking experiments with the aim to simulate the likely pathways of spilled oil in PGB during 2008–2012 in the area with monsoon-like climate. The first aim is to find preferable surface pathways of spilled oil in different seasons, as well as regions in the open-sea covered by the oil and risks of coastline contamination by the beaching of oil spills. With this aim, we compute the density of trajectories of the virtual oil particles released in a small area near Kozmino oil terminal and compute so-called dasymmetric maps Budyansky and Goryachev (2015); Prants et al. (2015) in two typical months with cardinaly different wind regime over the PGB area. These maps are designed to show accumulated density of trajectories of the surface tracers during February and August of every year from 2008 to 2012. We also plan to calculate monthly-averaged (2008–2012) relative concentrations of oil particles to compare the dispersion of oil in different months of a year. Another aim is, using the Lagrangian methods, to identify temporarily-coherent structures in the

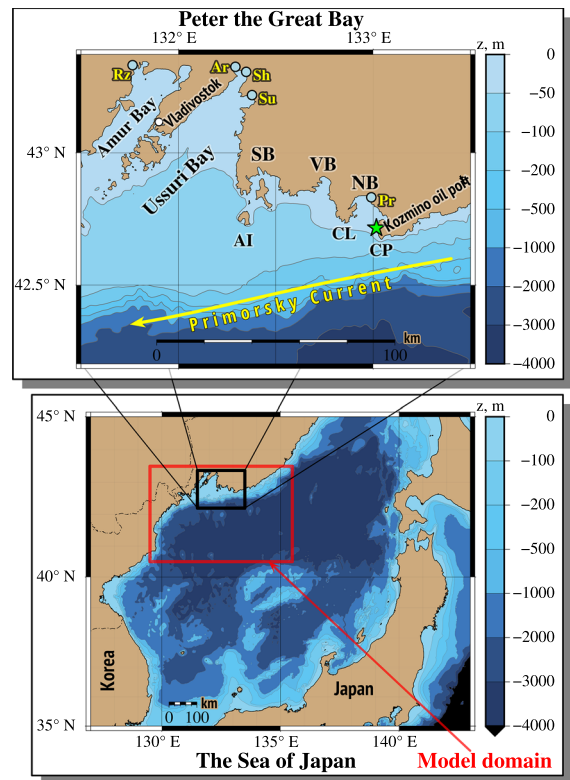


Figure 1

Bathymetric maps of Peter the Great Bay (top) and the Sea of Japan (bottom) with some geographic features. The computational domain is shown in the top panel with the 50, 100, 200, 500, 1000, 2000 and 3000 m isobaths. SB Strelok Bay, VB Vostok Bay, NB Nakhodka Bay, CL Cape Likhachev, CP Cape Povorotny, AI Askold Island. ★Kozmino oil port. Rz, Ar, Sh, Su and Pr are the mouths of Razdolnaya, Artemovka, Shkotovka, Sukhodol and Partizanskaya rivers

complex flow near the coast and in open sea which control the dispersal of oil slicks. With this aim, we compute the maps of the finite-time Lyapunov exponent Pierrehumbert (1991) that allow us to locate so-called Lagrangian fronts Prants et al. (2014a) and transport barriers Boffetta et al. (2001) that track the oil front and govern spill dispersal.

2. Common Features of Circulation in Peter the Great Bay

The seabed in PGB is a shallow shelf that breaks off abruptly along the steep continental slope down to the depth of 3 km (see Fig. 1). The major circulation features in the study area are the Primorsky Current

and cyclonic and anticyclonic eddies over the shelf. The Primorsky Current is a permanent feature of the general circulation that flows over the continental slope and affects the circulation in the shallow Amur and Ussuri bays which, in turn, affects circulation in smaller bays like Strelok, Nakhodka and Kozmino bays. In the upper layer, the Primorsky Current moves away from the coast in the southwestern direction. During the summer monsoon season, it is more stable and flows closer to the coast. A branch from the Primorsky Current enters Ussuri Bay and forms an anticyclonic circulation. During the winter monsoon season, the axis of the Current shifts off the coast Yurasov and Yarichin (1991). The mean speed is on the order of 10–20 cm/s in the surface and intermediate layers Isobe and Isoda (1997) and 5 cm/s in the deeper layer Takematsu et al. (1999).

Anticyclonic eddies drift southwestward along the northern periphery of the Primorsky Current from Cape Povorotny to Cape Gamov (see Fig. 1) Belinsky and Istoshin (1950). They have been found to contribute to the formation of anticyclonic circulation in Ussuri Bay, changing the hydrological parameters of the Bay Ladychenko and Lobanov (2013). Thus, circulation in the open waters and shallow bays of PGB is determined by the complex interaction of multiscale features such as basin geometry, bottom topography, wind, water exchange with the northwestern part of the Sea of Japan and river discharge. Instrumental measurements have shown that tides do not make a considerable contribution to circulation Shevchenko et al. (2017).

The speed of wind and its direction affect strongly on spilled oil drift, especially at the sea surface. The wind regime over PGB area is monsoon-like (www.meteoblue.com/en/weather/historyclimate/climatemodelled/vladivostok_russia_2013348). The cold northwest, west, and north winds from the continent prevail in the winter. All other directions account for less than 40% of frequency. In summer, south, southeast and southwest monsoon winds from the sea occur with the total frequency of about 30–40%. The high frequency of winds blowing from the sea is observed in the second half of August and in September. In the coastal zone, the orography affects the direction of air masses transport. Therefore, significant deviations from the main wind flow during

monsoon circulation can be observed over the coast. This deviation is especially noticeable in the warm season, when the direction becomes less stable with decreasing wind speed. Tropical cyclones, called typhoons, pass over the study area mainly from July to September. They impact strongly on the wind field and, consequently, on circulation in the sea.

For the case of coastal oil spill incidents, simulation with the conventional altimetric AVISO field is not reliable because the horizontal resolution of $1/4^\circ \times 1/4^\circ$ is not enough to resolve rapidly evolving submesoscale structures, and this product is absent at the distances smaller than ≈ 25 km away from the coast. Numerical models with high resolution or high-frequency radars may be the only viable option to study dispersal of oil spills near the shore and at submesoscale. In this study we use the Regional Ocean Modeling System (ROMS, www.myroms.org) with the horizontal resolution of 600 m.

3. Circulation Model

ROMS is a free-surface, nonlinear, primitive equation model featuring terrain-following coordinates in the vertical and advanced numerics Shchepetkin and McWilliams (2005). The model domain (Fig. 1), vertical and horizontal resolution, numerical schemes for vertical turbulence forcing, and bulk flux formulation were the same as in Fayman and Ostrovskii (2019), Prants et al. (2022) (see Table 1). The wind speed at the sea surface was obtained from the Daily ASCAT global wind field (6-hourly blended wind products with a spatial resolution of 0.25° in longitude and latitude over the global ocean).

Air pressure, incoming shortwave radiation, relative humidity, air temperature, precipitation and cloud cover were obtained from the NCEP-DOE AMIP-II Reanalysis. Daily SST, obtained from the Operational Sea Surface Temperature and Sea Ice Analysis (OSTIA), was used for the net heat flux correction Good and Fiedler (2020). According to this Analysis Donlon and Martin (2012), the sea ice in PGB is insignificant, and it was not taken into account in the calculations. Monthly sea surface salinity from World Ocean Atlas 2018 was used for

Table 1

The model domain (see Fig. 1) and parameters

Model domain	129.5° E–135.5° E; 40.5° N–43.5° N
Horizontal resolution	600 m
Vertical resolution	32 terrain-following vertical layers (vertical S-coordinate)
Vertical turbulence	Generic Length Scale scheme Umlauf and Burchard (2003)
Horizontal viscosity	Harmonic viscosity along constant potential density surfaces with the coefficient of 6 m ² /s
Horizontal diffusion	Harmonic diffusion along constant geopotential surfaces with the coefficient of 5 m ² /s
Atmospheric boundary layer	Bulk flux computation Fairall et al. (2003)
Pressure gradient	Finite volume Pressure Jacobian Lin (1997)

freshwater flux correction Zweng et al. (2019). Partizanskaya, Sukhodol, Shkotovka, Artemovka and Razdolnaya rivers flow into PGB. Daily mean data of the river discharge were obtained from the Automated Information System of State Monitoring of Water Objects (gmvo.skniivh.ru). Monthly mean data of the Tumen River discharge were obtained from the hydrological station in Quanhe Tian et al. (1999).

The lateral boundary conditions for temperature, salinity, velocity and sea surface height daily data were obtained from nesting the model into a Japan Coastal Ocean Predictability Experiment (JCOPE2) model dataset Miyazawa and Zhang (2009). The mixed radiation-nudging boundary condition, which assumes radiation conditions on outflow and nudging to a known exterior value on inflow, was imposed on all open boundaries for the 3D fields of temperature, salinity and velocity components. The Flather boundary condition was applied to the normal components of the barotropic velocity at a liquid boundary Flather (1976). The Chapman boundary condition was imposed to the surface height Chapman (1985). The model was run for the 20-year period (1999–2018), starting from the initial conditions generated by interpolation of the JCOPE2 fields on January 1, 1999. The simulated ocean fields were saved every hour. The Message-Passing Interface programming was used to provide faster and more

powerful problem-solving with the help of a parallel computing.

When simulating the spilled oil dispersal, adequate representation of the currents in the upper 0–5 m layer is crucial. In warm seasons, the ROMS reproducibility of current variability has been verified by comparing simulation results with regular CTD data in 25 oceanographic expeditions conducted in PGB from May to September in 2001–2016 by the Far Eastern Regional Hydrometeorological Research Institute (FERHRI, Vladivostok). The results of ROMS simulations have been found to be in a good agreement with the results of diagnostic simulation based on these CTD measurements. In particular, ROMS has been able to reproduce the observed current field and major features like eddies and currents on a monthly mean basis both in the warm and cold seasons.

The model has shown a good performance including the reproducibility of anticyclonic eddies regularly generated past the Cape Povorotny Fayman et al. (2019) and their southwestward advection by the Primorsky Current. In the cold season, ROMS has shown good results in simulating various physical processes in PGB comparing simulation results with the CTD data from an Aqualog profiler and bottom stations Fayman and Ostrovskii (2019); Prants et al. (2022).

4. Lagrangian Methods

In the Lagrangian approach, transport and mixing processes are studied by following passive particles (tracers). Trajectories of particles are computed by solving advection equations which in our case are two dimensional:

$$\frac{d\lambda}{dt} = u(\lambda, \varphi, t), \quad \frac{d\varphi}{dt} = v(\lambda, \varphi, t), \quad (1)$$

where φ and λ are latitude and longitude, respectively, and u and v are the angular zonal and meridional components of the velocity field in the upper model layer at the location of the particle, respectively. Angular velocities u and v are measured in arc minutes per day and are related to linear velocities U and V in cm/s by the ratio:

$$u = \frac{0.864}{1.853} \frac{1}{\cos \varphi} U, \quad v = \frac{0.864}{1.853} V. \quad (2)$$

The advection equations (1) in terms of angular velocities have the simplest form Prants (2014). The Lagrangian trajectories were computed by integrating (1) with the fourth-order Runge–Kutta scheme with the constant time step of 86.4 s, a bicubic spatial interpolation and time interpolation by Lagrangian polynomials of the third order.

It has been reported that more than 90% of oil stays in the 0–3 m surface layer Guo and Wang (2009). Therefore, we assume that oil remains at the surface and that the vertical movement of individual particles is neglected during the short integration period of 4–6 days. The processes of sedimentation to the bottom, degradation and the formation of oil clots take more time Korotenko et al. (2003). Therefore, we take into account oil evaporation and biodegradation processes only with the half-lifetimes T_{evp} and T_{bio} which have been estimated to be 25 h and 250 h, respectively Varlamov et al. (1999); Ono and Ohshima (2013).

Integrating equations of advection (1) with many thousands of particles, we identify advective pathways and their variations in different seasons and years. With the task to determine the potential pathways of oil after a hypothetical spill from the Kozmino oil terminal, we did not take into account turbulent diffusion in the equations of motion. To test that the variability of the velocity field is much more important to determine the pathways of spilled oil than a small-scale turbulence, we have carried out a large number of numerical experiments adding a random component to the model velocity in the upper layer. The adding of a stochastic component did not lead to cardinal changes in the shape of the oil patches launched in different seasons. During the first two-five days after launching, the oil patches with a stochastic component only slightly blurred as compared with the patches without a stochastic component (see Fig. 1S in Supplementary material). Similar results have been obtained by other authors who have studied a sensitivity of location of Lagrangian coherent structures and fronts to errors by adding a random noise to the model or altimetric velocity field (see, e.g., Harrison and Glatzmaier

2012; Hernández-Carrasco et al. 2011; Keating et al. 2011). They have shown that the location and shape of coherent structures with noise were similar, albeit blurred, to structures without noise.

We consider evaporation and decay in a simplified manner. These processes depend on oil components, temperature, wind speed and biomass Guo and Wang (2009). In the case of a real incident, a high-accuracy parametrization is needed for more realistic oil spill simulation. However, it is out of the scope of our study devoted to simulation of likely pathways of oil and to analysis of oceanographic features and material structures that shape spilled oil evolution and affect these pathways.

In majority of the particle-tracking experiments, $N = 90,000$ particles, evenly spaced in a small area $42.7^\circ \text{ N} - 42.725^\circ \text{ N}$, $132.98^\circ \text{ E} - 133.025^\circ \text{ E}$ ($3.7 \times 2.8 \text{ km}$) around the Kozmino oil port (see Fig. 1) are deployed every hour from 00:00 to 23:00 GMT on the first day of every month. We calculate the tracer concentration $C_i(t)$ at time t (in hours) for the i -th particle. The initial value of $C_i(0)$ is set to be unity and $C_i(t)$ is calculated as $C_i(t) = e^{-(k_{\text{evp}} + k_{\text{bio}})t}$, where the values of the coefficients k_{evp} and k_{bio} are defined by $\log(2)/T_{\text{evp}}$ and $\log(2)/T_{\text{bio}}$ using half-lifetime $T_{\text{evp}} = 25 \text{ h}$ and $T_{\text{bio}} = 250 \text{ h}$. Particle concentrations are calculated until 00:00 by the fifth day of the month in which the particles were launched. Because of this, the value of t and, as a consequence, the concentrations differ for particles launched at early and late hours. The particles, launched at 00:00 on the first day of the corresponding month for which $t = 96$, have the smallest concentration.

The simulation results in Sect. 5 show plots of the concentration which were computed as follows. The study area $42.3^\circ \text{ N} - 43.4^\circ \text{ N}$, $131.7^\circ \text{ E} - 133.5^\circ \text{ E}$ was divided into 300×300 bins with the size of 667 m for latitude and 360 m for longitude. At the first stage, the relative concentration was calculated in each bin $C(\%) = \sum C_i(t)/N \times 100$, where $N = 2,160,000$ is the total number of released particles, and $\sum C_i(t)$ is the sum of the concentrations found in the bin at the moment of time t . Such summation was done for every month and every year separately. At the second stage, the monthly-averaged relative concentration was calculated for each bin summing

$C(\%)$ in the same months in 2008–2012 and diving the total sum by 5 years. The monthly-averaged relative concentration is a dimensionless quantity defining the fraction of oil particles (taking into account the degradation of oil over time) in different regions of the study area. That allows us to compare the dispersion of oil in different months of a year. If a particle enters a coastal cell of the interpolated velocity field, it either remain at the coast (the beaching effect) for a while or leave the coast under the action of the suitable current field. Finally, the relative concentration is averaged over five years.

To analyze the dispersal pathways, Lagrangian methods are especially useful. Besides the direct integration of advection equations for passive particles in a prescribed velocity field, they also include special techniques on calculation Lagrangian fronts which transports tracers. By definition Prants (2014), the Lagrangian front is a structure with the (local) maximum gradient of a Lagrangian indicator, i.e., it is a boundary between areas with very different values of this indicator. To detect these frontal structures, controlling trajectories of tracers and therefore forecasting transport pathways of a contaminant, we use here the finite-time Lyapunov exponent Λ Pierrehumbert (1991). Λ is a finite-time average of the divergence/convergence rate of initially close-by particles that is calculated here by the method proposed by Prants et al. (2011). The equations (1) are linearized near a given trajectory to obtain a set of equations for infinitesimal deviations from it. Then, the 2×2 evolution matrix is calculated to find its largest singular value $\sigma_1(t, t_0)$, which shows how much an initially small deviation increases. The ratio of the logarithm of the maximal possible stretching in a given direction to the integration time interval $t - t_0$ gives the value of the finite-time Lyapunov exponent:

$$\Lambda = \frac{\ln \sigma_1(t, t_0)}{t - t_0}. \quad (3)$$

The values of Λ are computed backward in time for six days for a large number of oil particles distributed homogeneously over the study area starting at the beginning of every hour of every day in every month in 2008–2012. Then Λ values are plotted on a geographic map of the study area providing us with

hourly Lyapunov maps. The curves of the (locally) maximum values of Λ (“ridges”) approximate attracting manifolds when integrating the advection equations backward in time (see, e.g., Haller 2002). These manifolds are material lines consisting of the particles diverging from each other in the course of time with the maximal rate. That is why they can be approximated by the “ridges” in the Lyapunov field. The prominent “ridges” with large values of Λ are Lagrangian fronts that evolve in time and control transport processes Prants (2022).

Cyclonic and anticyclonic eddies are regular features in PGB which occur both in the warm and cold seasons. It is expected that they could play an important role in dispersal of oil spills in PGB. So, it is necessary to have an effective method to identify and track submesoscale and mesoscale eddies. First of all, we compute the locations of stationary points with zero velocity and record them every hour. The standard stability analysis is then performed to specify the stagnation points of elliptic and hyperbolic type (for details see Prants et al. 2014b, 2017). The stable elliptic points (triangles on the maps) are located at the centers of eddies where rotation prevails over deformation. The birth of an eddy is signaled by the appearance of an elliptic point, whereas its disappearance signals the decay of an eddy. The hyperbolic points (crosses on the maps), where deformation prevails over rotation, are located mostly between eddies. They have associated repelling stable and attracting unstable manifolds.

5. Results of Simulation and Discussion

5.1. Particle-Tracking Simulation

The reproduction of the current field including its variability is the most important for oil spill simulation. The results of particle-tracking experiments strongly depend on oceanographic situation in small bays and the open part of PGB on the day of a hypothetical accident and after that. The current field at the surface, in turn, strongly depends on wind conditions. The monsoon-like wind regime over PGB area www.meteoblue.com/en/weather/historyclimate/climatemodelled/vladivostok_russia_2013348 is one

of the key factors governing surface spilled oil dispersal.

To estimate possible pathways of spilled oil after a deployment from the Kozmino oil terminal, we computed the so-called dasymetric maps Budyansky and Goryachev (2015); Prants et al. (2015) for two months with cardinally different wind regime over the PGB area. The region in Fig. 2 was divided into 300×300 bins with the size of 667 m for latitude and 360 m for longitude. 40,000 tracers were released in the surface layer from a small area near the port with the size of 3.7×2.8 km every day at 00:00 GMT during February and August of every year from 2008 to 2012. The advection equations (1) were integrated forward in time to count hourly how many times v the oil particles visit each bin during February and August in 2008–2012. The counting time for each trajectory was 6 days.

The dasymetric maps in Fig. 2 show not a collection of particle's trajectories but an accumulated density of particle's traces in the logarithmic scale in every bin by white-to-black gradation. In the logarithmic scale, even a small color contrast means a considerable difference in the density of particle's traces that is higher near the source and decays with distance from the source. However, the color contrast between the density of particle's traces near the

source and at a distance is not extremely large due to the rapid removal of oil particles from the coast to the open sea by the Primorsky Current. In other words, these maps show preferable pathways of oil particles in PGB during a short period of time.

In February, the prevailing north/northwest winds cause predominantly southwestward drift of the oil particles and their advection to the open sea by the Primorsky Current. In August, the prevailing south/southeast winds favor a dispersion of the particles in the area covering the smaller bays in PGB, including the Nakhodka, Vostok, Strelok and Ussuri bays with a high risk of contamination of the coastal recreation zones.

The relative tracer concentration at the surface was computed as it was described in Sect. 4. $N = 90,000$ virtual oil particles were released every hour within 24 hours with the start at the beginning of the first day of every month. The concentration was averaged for every month in 2008–2012 and plotted on the geographic map in Figs. 3 and 4 by the beginning of the fifth day after the deployment.

As it was pointed out in Sect. 2, the permanent circulation feature in the study area is the Primorsky Current schematically shown in (Fig. 1). Its speed varies depending on the season, but all the year it flows approximately in the same southwestward

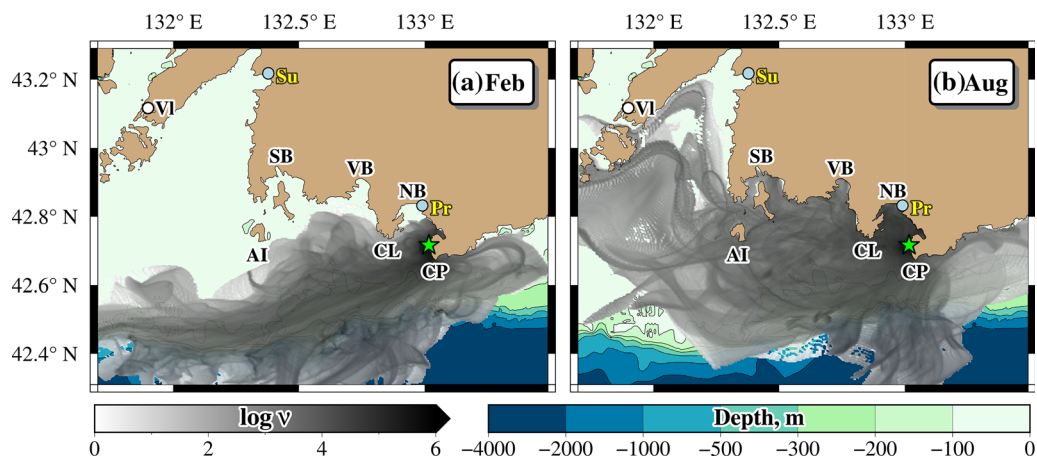


Figure 2

The dasymetric maps show the accumulated density of trajectories of the surface tracers released from the Kozmino oil terminal (the star) **a** in February and **b** in August months with prevailing winds from the continent and from the sea, respectively. The data are accumulated within six days after the release and shown in the logarithmic scale. For more details see the main text. The abbreviations are the same as in caption to Fig. 1

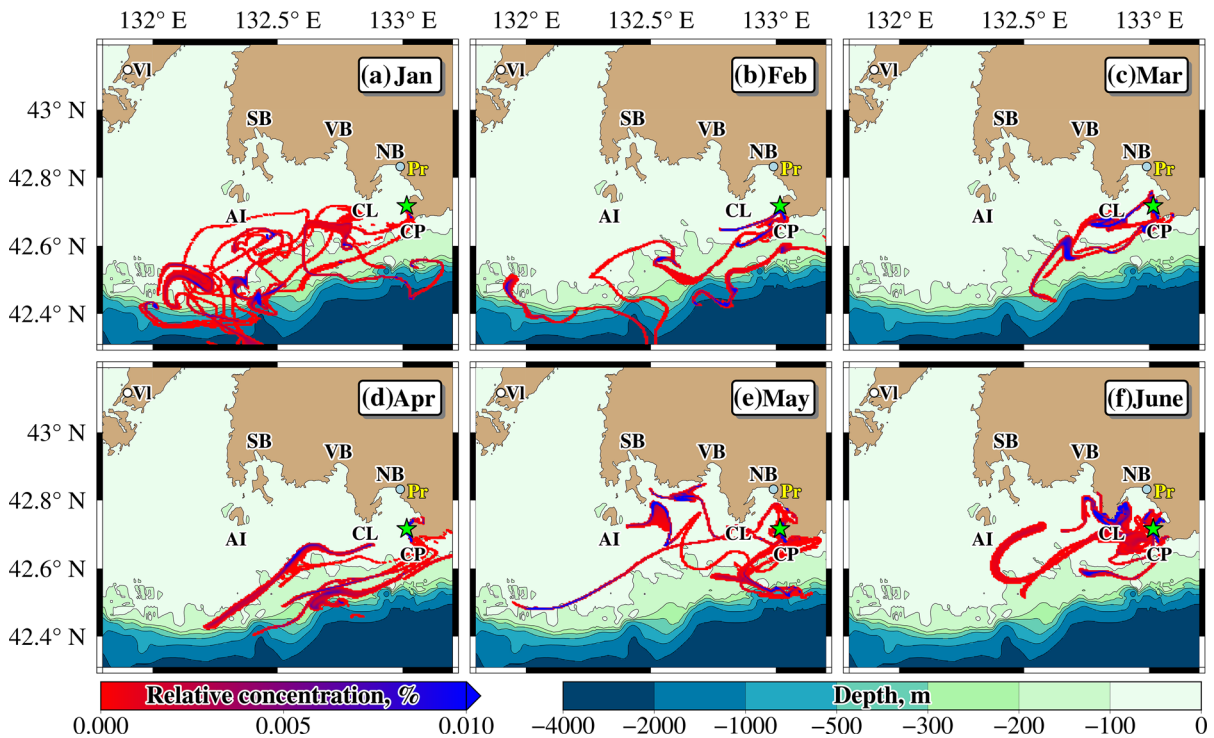


Figure 3

Monthly-averaged (2008–2012) tracer concentrations are shown at 00:00 GMT of the fifth day after the deployment of particles from a small area near the Kozmino oil port (the green star). For details, see the main text. The bars show relative concentration in the upper layer and the depth in the study area. The abbreviations are the same as in caption to Fig. 1

direction. However, particle-tracking experiments in 2008–2012 have shown that configuration of the calculated oil slicks, their shape and distance from the coast are very different in different months of a year (see Figs. 3 and 4).

We distinguish three main scenarios of surface propagation of the spilled oil in the first days after the incident. In the first scenario, the spilled oil moves fast away from the coast. That occurs mainly in the cold season when strong north/northwest winds from the continent favor the removal of tracers from the source. In the second scenario, tracers remain near the coast, at least, for the first four days after the incident. It occurs often in summer with prevailing south/southeast winds from the sea which create conditions for blocking propagation of spilled oil from the coast to the open sea. The third scenario is an intermediate one with the oil spill dispersal away from the coast but not too far away from the Kozmino oil terminal as compared to the first scenario. That

occurs predominantly at weak winds or when the wind changes fast its direction.

Selection of three scenarios in accordance with displacement of the oil slicks away from the coast is, of course, conditional. It's more important that in the warm season the concentration of the spilled oil is typically larger near the coast as compared to the cold season. Moreover, the oil slicks propagate predominantly westward in the "warm" months covering the coast of the Nakhodka and Vostok bays (see also the dasymetric map in August in Fig. 2). In the cold season, the southwestward drift of the oil slicks is more pronounced (see also the dasymetric map in February in Fig. 2).

The results obtained in this section show that the direction and speed of wind have a significant impact on the surface transport of the spilled oil. The Lagrangian analysis in the next section provides a deeper insight into the reasons of the behavior of oil slicks in different seasons.

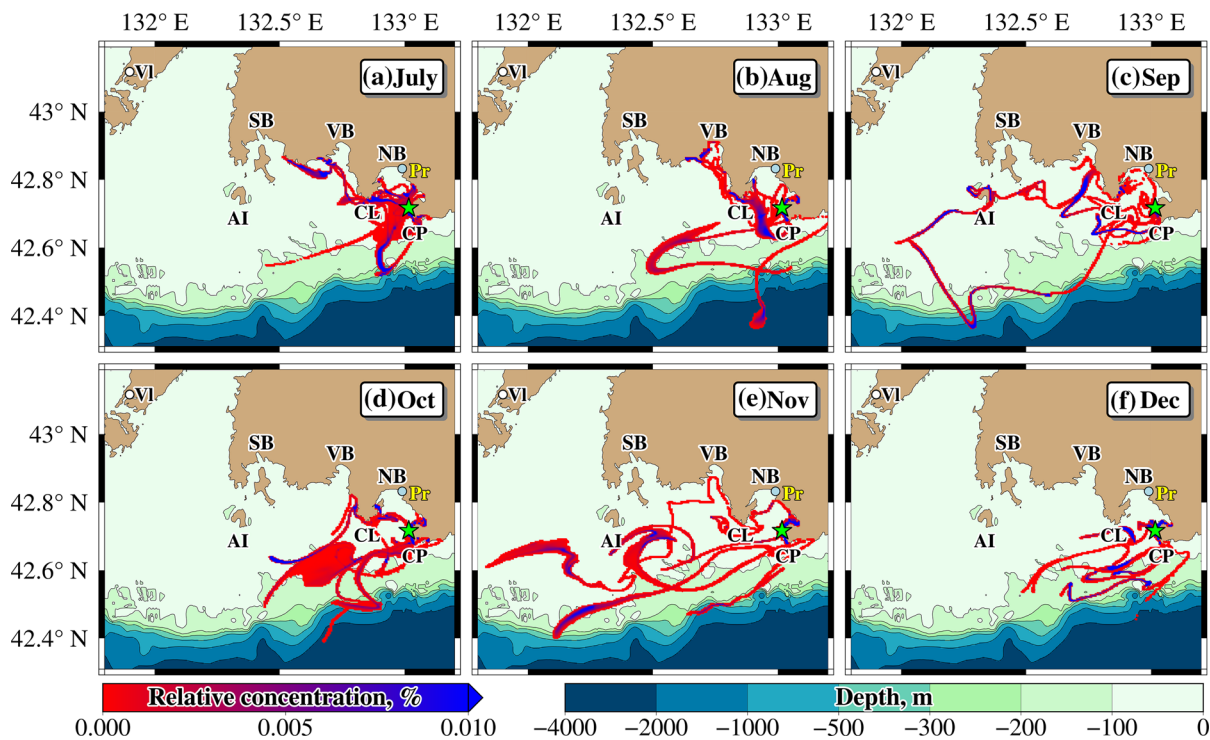


Figure 4
The same as in Fig. 3 but for July – December

5.2. Lagrangian Fronts Detection

In this section we explain why the spilled oil is advected just after the deployment in a distinct manner in different months of a year. With this aim, we computed the Lyapunov maps for 90,000 particles distributed homogeneously over the study area starting at the beginning of every hour of every day in every month in 2009. The procedure was explained in Sect. 4.

The inspection of 8760 Lyapunov maps allowed us to conclude that the dispersal of the spilled oil is controlled by strong Lagrangian fronts which are approximated by dark “ridges” on the maps with the large values of the finite-time Lyapunov exponent Λ (3). These “ridges” are shown by blue elongating bands in Figs. 5, 6, 7 consisting of a number of material lines each of which, by the definition of Λ (3), is a collection of particles diverging from each other with the maximal rate in the course of time. The Lagrangian fronts evolve in

the course of time and exist for a finite period of time in oceanic flows.

The finite-time Lyapunov exponent is a quantitative measure of chaos in fluid flows. It is more important for the problems of oil dispersion that the “ridges” in the Lyapunov field are Lagrangian fronts which minimize advection of oil particles across the front and maximize advection along the front. The tracers from outside cannot cross the front transversally because they consisted of material lines. They can do that only due to a small-scale diffusion that does not lead to cardinal changes in the shape of the oil patches during the considered comparatively short period of time (see Fig. 1S in Supplementary material). It is expected that the Lagrangian fronts, formed near coast just after deployment of oil particles, control evolution of the oil patch at the first stage. As the front moves away from the coast, a patch follows it, deforming in accordance with the deformation of the front. This advective process can be complicated by the presence of other Lagrangian fronts in the study area.

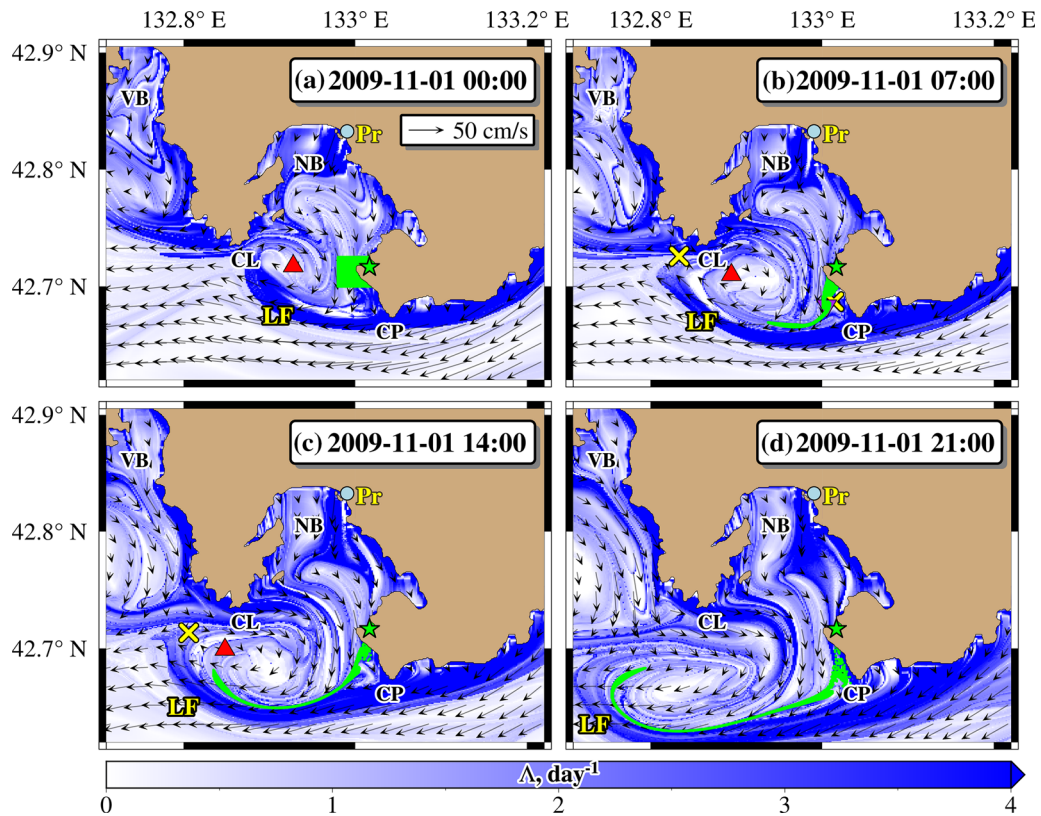


Figure 5

The finite-time Lyapunov exponent maps show snapshots of the evolving oil spill (green particles) with Lagrangian fronts and surface current field overlaid. The evolving front LF shapes the spilled oil and simultaneously acts as a transport barrier. The tracers were released at 00:00 GMT on November 1, 2009. The red triangle and yellow cross show elliptic and hyperbolic points, respectively. The surface current field is shown by arrows. The Δ values are given in day^{-1} . The abbreviations are the same as in caption to Fig. 1

This speculations are illustrated by the Lyapunov map in Fig. 5 with a moving Lagrangian front which transports the spilled oil and simultaneously acts a transport barrier. The passive tracers, imitating oil particles in the surface layer, were released at the oil spill site at 00:00 GMT on November 1, 2009 (Fig. 5a). The strong Lagrangian front, formed before this date to the south of the Kozmino port, initially blocked the spread of the oil slick away from the coast due to the wind from the sea. By the beginning of November 1, wind direction changed to the north wind and then to the northwest/west wind (see Table in the Supplementary Material). The location of this front deliniates an attracting unstable manifold associated with two yellow hyperbolic points in Fig. 5a. This front initially pushed the oil westward. As the front moved, it attracted and stretched the oil

slick transporting oil around the anticyclonic eddy with the center at 42.45° N , 132.54° E (the red triangle in Fig. 5a). This eddy gradually drifted to the open sea advecting the spilled oil around its periphery (Fig. 5b–d). The oil slick did not directly follow the surface current oriented southwestward but drifted in a more complicated way following the nearest strong front. Therefore, Lagrangian fronts attract the spilled oil, stretch the oil slick and act as transport barriers. The deep reason of that is the presence of attracting unstable manifolds in chaotic flows which are approximated by the “ridges” in the Lyapunov field (see, e.g., Haller 2002).

In the preceding section, we selected three scenarios of propagation of the spilled oil in the study area. Based on the Lyapunov maps, computed in 2009, we analyze now the oil spill dispersal from

the Lagrangian point of view. The first scenario with fast removal of spilled oil from the source in the cold season with prevailing north winds is illustrated in Fig. 6 where the evolution of the surface oil slick, deployed at 00:00 GMT on January 1, 2009 (Fig. 6a) is shown for the first three days after the deployment in the field of the finite-time Lyapunov exponent Λ . A strong Lagrangian front formed by the end of the first day after the deployment. The tracers have been gradually distributed along it (Fig. 6b). Due to the strong northwest/west winds with the speed of around 10–12 m/sec (see Table in the Supplementary Material), the front drifted fast away from the coast gradually stretching the oil slick (Fig. 6c). By the

beginning of the fourth day, the perimeter of the slick increased significantly, the slick has been stretched and transported away from the coast, and its head split following two different fronts (Fig. 6d).

In the second scenario the behavior of the spilled oil is cardinally different. This scenario often occurs in the warm season with prevailing winds from the sea. Figure 7 illustrates the second scenario where the oil slick was deployed at 00:00 GMT on June 1, 2009. Due to the easterly/southeast winds (see Table in the Supplementary Material), a strong Lagrangian front formed by the beginning of June 1st (Fig. 7a). The front drifted then to north creating a transport barrier which prevented spread of spilled oil

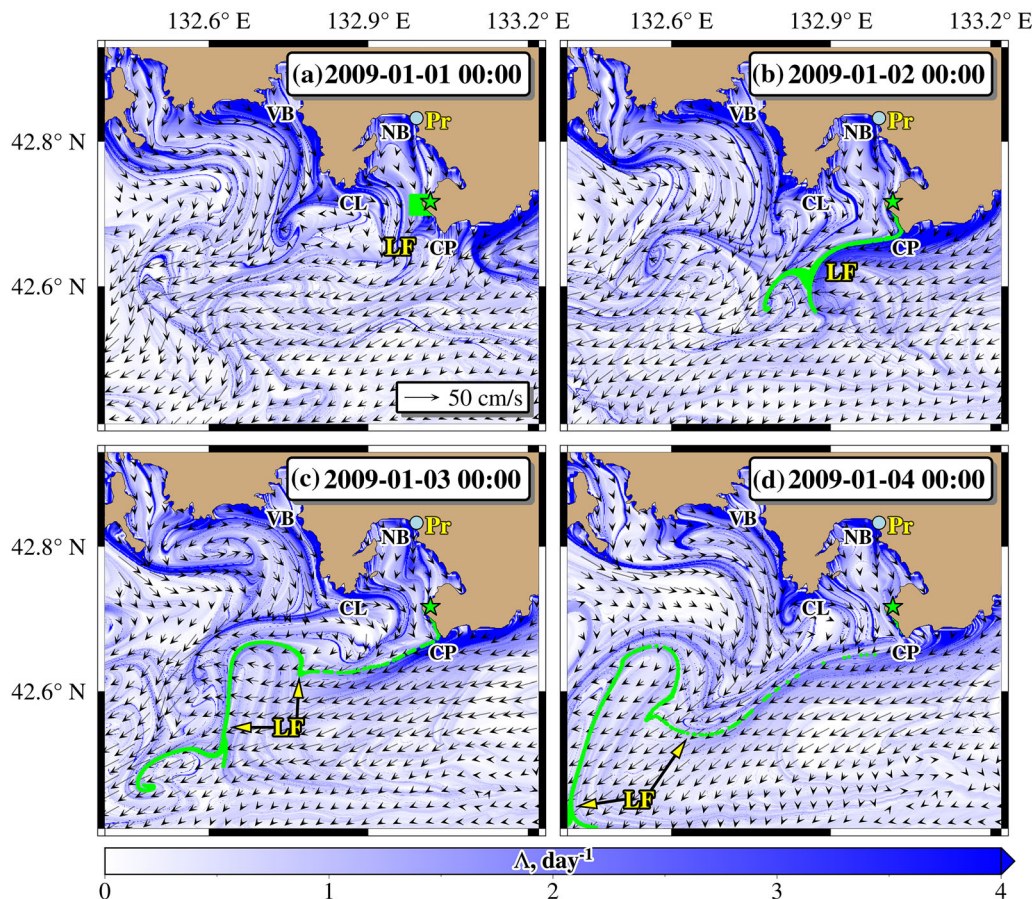


Figure 6

Lyapunov maps illustrate the first scenario with fast removal of the spilled oil from the coast in the cold season. The oil slick (green particles), released at 00:00 GMT on January 1, 2009, follows the Lagrangian front (LF) drifting away from the coast. The abbreviations are the same as in caption to Fig. 1

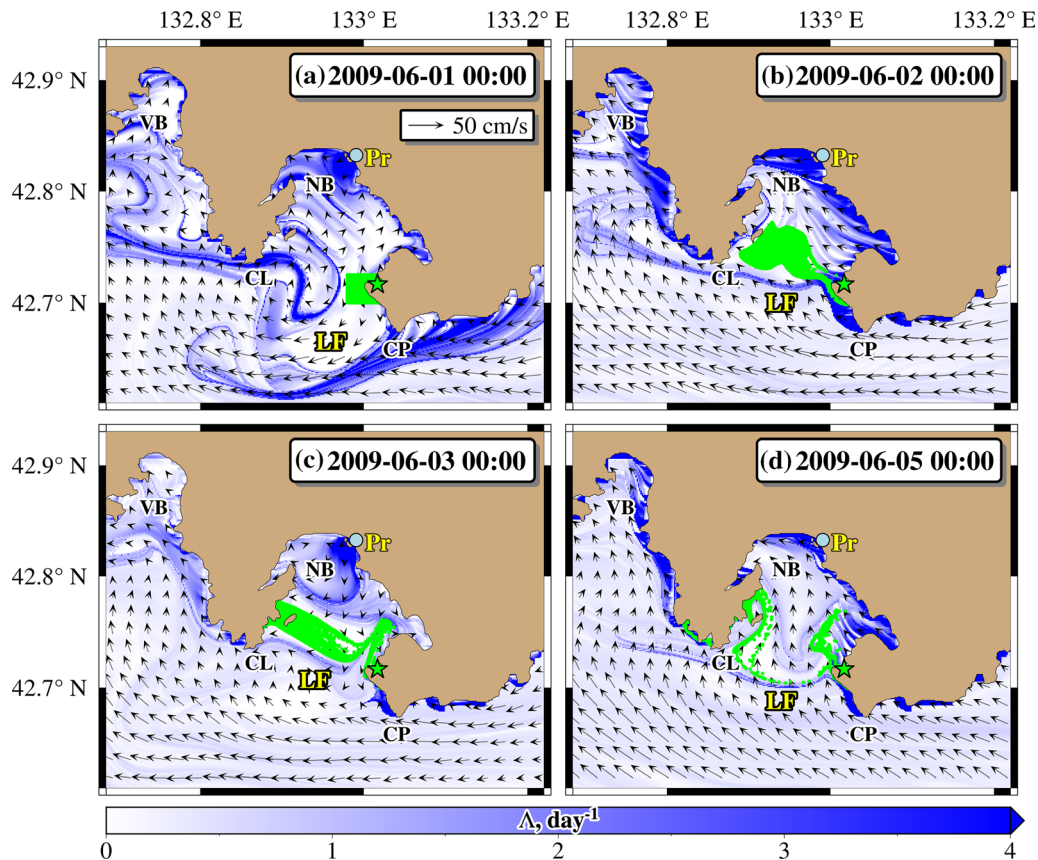


Figure 7

Lyapunov maps illustrate the second scenario where the spilled oil remained near the coast for the first days after the deployment at 00:00 GMT on June 1, 2009. The drifting Lagrangian front (LF) acts as a transport barrier preventing spread of the oil slick (green particles) to the open sea. The abbreviations are the same as in caption to Fig. 1

to the open sea (Fig. 7b–d). The tracers from outside could not cross this near-coastal front transversally because it consisted of material lines. The front existed, at least, for 5 days after the deployment, and the oil slick has stretched gradually along the Nakhodka Bay coast.

The third scenario is illustrated in Fig. 8 where the evolution of the surface oil slick, deployed at 00:00 GMT on October 1, 2009 is shown in the field of the finite-time Lyapunov exponent. October typically is the quietest month in the area with weak and multidirectional winds. A Lagrangian front was initially oriented almost zonally (Fig. 8a) due to the south/southwest wind (see Table in the Supplementary Material) preventing the oil spill dispersal to the central part of PGB (Fig. 8b). After two days, the

wind direction changed to the northwest/west one, and the front begun to drift to the southwest (Fig. 8c). Then the wind direction changed once again to the west/southwest one and lead to almost zonal orientation of the front (Fig. 8d). The major part of the passive tracers of the initial oil slick has been gradually distributed along the front. A smaller part remained near the coast in the Nakhodka Bay. This front drifted away from the coast gradually stretching the oil slick. By the end of the fifth day after the deployment, the oil slick reached the central part of PGB (Fig. 8d).

Accidental oil spills require an immediate effective response that ideally requires additional information on the future spread of oil slicks. Lagrangian fronts evolve in time and they do that

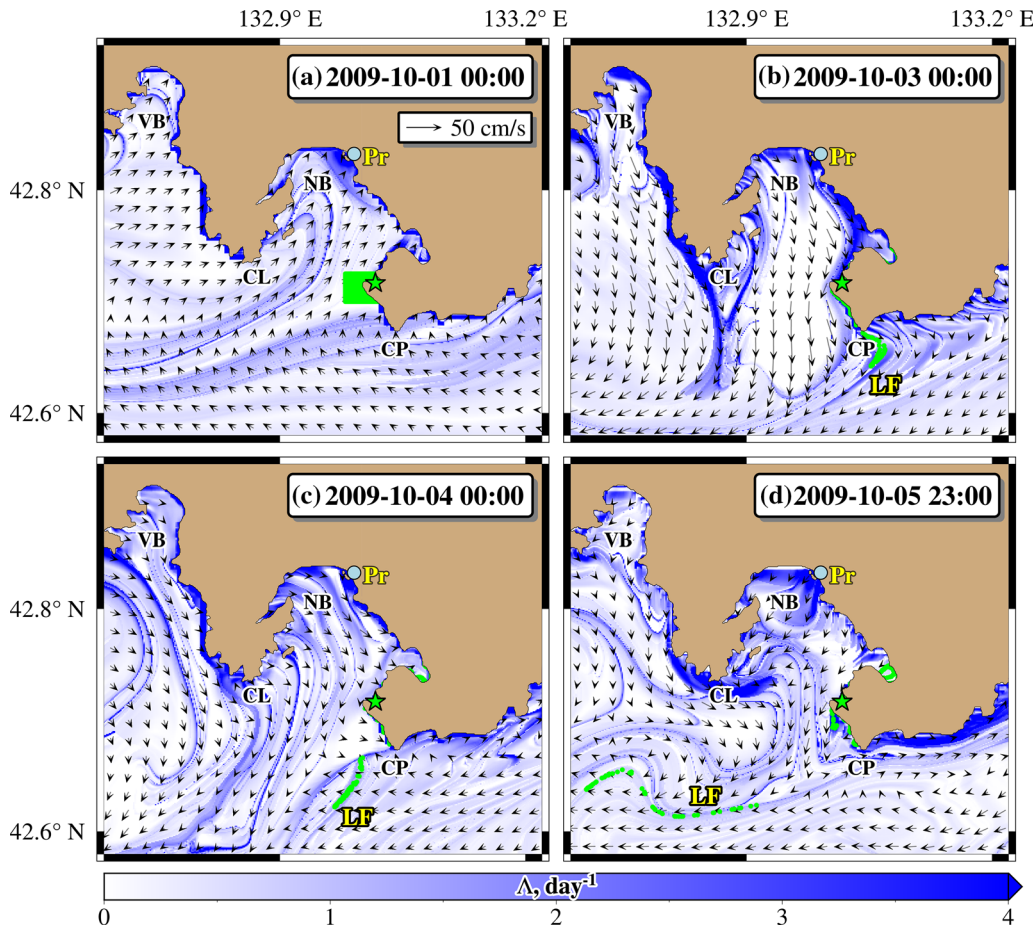


Figure 8

Lyapunov maps illustrate the third scenario where the spilled oil remained near the coast for the first two days after the deployment at 00:00 GMT on October 1, 2009 and then it began to remove away from the coast following the evolving Lagrangian front (LF). The abbreviations are the same as in caption to Fig. 1

sometimes in a complicated manner (see Figs. 6, 7 and 8). The possibility of anticipating the future front position would be very important when estimating the oil spill dispersal. Knowing the position of Lagrangian fronts in a region, where an oil spill has occurred, helps to forecast the location of oil slicks. The Lagrangian approach can help with this because Lyapunov maps, in principle, allow us to predict the position of the prominent “ridges” in the future on timescales of the order of the inverse of the Lyapunov exponent, based on near real-time velocity field alone, i.e., without the need for velocity forecast Olascoaga and Haller (2012).

A method for predicting the drifting speed of Lagrangian fronts has been elaborated by Fifani and Baudena (2021). It is based on a theoretical property of the flux across Lagrangian fronts defined as “ridges” of finite-time Lyapunov fields. Shadden et al. (2005) showed that under general conditions this flux can be considered as small and in most cases negligible for well-defined “ridges”. Whenever a “ridge” appears to be transverse to a smooth velocity field, a sufficient condition for maintaining a zero flux is to impose a local displacement of the “ridge” by the component of the velocity field orthogonal to it Fifani and Baudena (2021). The drifting speed of Lagrangian fronts at a given point is calculated as the

orthogonal projection of the current velocity vector on the orthogonal direction to the corresponding “ridge”. This method is applied to all the points over the front, providing its future displacement after a defined short-time period.

However, the applicability and effectiveness of this forecast method depend on the area where an oil spill has occurred. In the open sea, the maximum values of the finite-time or finite-scale Lyapunov exponents have been found to be less than 0.4 days^{-1} (see, e.g., Fifi and Baudena 2021), allowing to predict the position of Lagrangian fronts on time-scales of the order of Λ^{-1} , i.e., theoretically no more than for four days ahead. In large bays, the maximum Λ values could reach 0.8 days^{-1} Budyansky et al. (2022). In our case, the maximum Λ values reach 4 days^{-1} near the coast making the forecast problematic. Recalling that Λ is a finite-time average of the divergence rate of initially close-by particles (see Sect. 4), it is obvious that such large values of Λ near the coast are explained by fast divergence of the particles moving away from the coast and the particles remained near the coast. However, in the open part of PGB the values of Λ for prominent “ridges” ranges from 0.5 to 1 days^{-1} allowing to predict the position of the corresponding Lagrangian fronts on the timescale of 1–2 days. This possibility can support management and prediction tools for oil spills when every day is important in a clean-up of oil spills.

6. Conclusion

Using the retrospective ROMS-based velocity field with the horizontal resolution of 600 m, we simulated the surface spread of a hypothetical oil spill deployed from one of the most important oil outlets in Russia, the Kozmino port near Vladivostok. The results of Lagrangian particle-tracking experiments with a large number of tracers were shown by the relative concentration averaged in 2008–2012. They allowed us to find preferable surface pathways of spilled oil in PGB in different seasons, as well as regions in the open-sea covered by the oil and risks of coastline contamination by the beaching of oil spills. The monsoon-like wind regime over the PGB area

was shown to play the important role in the surface spread of oil. Applying a special Lyapunov technique, we could identify Lagrangian temporally-coherent structures, Lagrangian fronts, which track the oil front and govern spill dispersal. As a Lagrangian front drifts, the oil slick moves along its pathway. At the same time, the front acts as a transport barrier preventing cross-frontal transport of oil. The Lyapunov maps might serve not only as an efficient tool for use in oil spill emergency response planning but also to predict changes in the oil patterns over a few days on the basis of near-real-time information alone.

Three main scenarios of propagation of the spilled oil have been found. In the first one, the spilled oil drifts fast away from the coast due to strong north/northwest winds and specific distribution of the Lagrangian fronts in the study area which favor the removal of oil away from the source. That occurs mainly in the winter and spring months. In the second scenario, oil remains near the coast. It occurs typically in the warm season with prevailing south/southeast wind that creates conditions for appearance of transport barriers blocking surface propagation of spilled oil away from the coast to the open sea. If so, the oil should “seek” for gaps between different transport barriers to enter the open sea between them. The third scenario is an intermediate one with the dispersal of the spilled oil away from the coast but not too far away from the Kozmino oil terminal as compared to the first scenario.

The ROMS-based hourly Lagrangian maps might serve as an efficient tool for use in oil spill emergency response planning. The aim of emergency response planning is to reduce the response time, to forecast changes in the oil patterns and to increase the effectiveness and efficiency of the response actions. The knowledge of location of the Lagrangian fronts/barriers in various parts of PGB and of rapid pathways of oil at the time of real incidents opens a new way towards developing a simulation-based technology that could use this knowledge for the reduction of environmental risks. The key benefit of the proposed Lagrangian methods is an increase in the time for an adverse impact of oil spills to reach the coastal zone.

Author Contributions All authors contributed to the study conception and design. Material preparation, data collection and analysis were performed by SP, MB, PF, MU and AD. The first draft of the manuscript was written by Sergey Prants and all authors commented on previous versions of the manuscript. All authors read and approved the final manuscript.

Funding

The work was supported by the Russian Foundation for Basic Research (RFBR, project No. 20-05-00124A) with the help of a high-performance computing cluster at the Pacific Oceanological Institute of the Russian Academy of Sciences (State Task No. 121021700341-2).

Declarations

Conflict of interest The authors have no relevant financial or non-financial interests to disclose.

Publisher's Note Springer Nature remains neutral with regard to jurisdictional claims in published maps and institutional affiliations.

Springer Nature or its licensor (e.g. a society or other partner) holds exclusive rights to this article under a publishing agreement with the author(s) or other rightsholder(s); author self-archiving of the accepted manuscript version of this article is solely governed by the terms of such publishing agreement and applicable law.

REFERENCES

- Abdalla, S., Kolahchi, A. A., et al. (2021). Altimetry for the future: Building on 25 years of progress. *Advances in Space Research*, 68(2), 319–363. <https://doi.org/10.1016/j.asr.2021.01.022>.
- Amir-Heidari, P., & Raie, M. (2019). Response planning for accidental oil spills in Persian Gulf: A decision support system (DSS) based on consequence modeling. *Marine Pollution Bulletin*, 140, 116–128. <https://doi.org/10.1016/j.marpolbul.2018.12.053>.
- Belinsky, N. A., & Istoshin, Y. V. (1950). Primorskoe current as observed in expedition of the boat “Rossinante” in 1936. *Trudy Centralnogo Instituta Prognozov*, 17, 132–143 ([in Russian]).
- Boffetta, G., Lacorata, G., Redaelli, G., & Vulpiani, A. (2001). Detecting barriers to transport: A review of different techniques. *Physica D: Nonlinear Phenomena*, 159(1–2), 58–70. [https://doi.org/10.1016/S0167-2789\(01\)00330-X](https://doi.org/10.1016/S0167-2789(01)00330-X).
- Budyansky, M. V., Goryachev, V. A., et al. (2015). Role of mesoscale eddies in transport of Fukushima-derived cesium isotopes in the ocean. *Deep Sea Research Part I: Oceanographic Research Papers*, 96, 15–27. <https://doi.org/10.1016/j.dsr.2014.09.007>.
- Budyansky, M., Fayman, P., Uleysky, M., & Prants, S. (2022). The impact of circulation features on the dispersion of radionuclides after the nuclear submarine accident in Chazhma Bay (Japan Sea) in 1985: A retrospective Lagrangian simulation. *Marine Pollution Bulletin*, 177, 113483. <https://doi.org/10.1016/j.marpolbul.2022.113483>.
- Chapman, D. C. (1985). Numerical treatment of cross-shelf open boundaries in a barotropic coastal ocean model. *Journal of Physical Oceanography*, 15(8), 1060–1075. [https://doi.org/10.1175/1520-0485\(1985\)015<1060:ntocso>2.0.co;2](https://doi.org/10.1175/1520-0485(1985)015<1060:ntocso>2.0.co;2)
- Ciappa, A., & Costabile, S. (2014). Oil spill hazard assessment using a reverse trajectory method for the Egadi marine protected area (Central Mediterranean Sea). *Marine Pollution Bulletin*, 84(1–2), 44–55. <https://doi.org/10.1016/j.marpolbul.2014.05.044>.
- Donlon, C. J., Martin, M., et al. (2012). The operational sea surface temperature and sea ice analysis (OSTIA) system. *Remote Sensing of Environment*, 116, 140–158. <https://doi.org/10.1016/j.rse.2010.10.017>.
- Duran, R., Beron-Vera, F. J., & Olascoaga, M. J. (2018). Extracting quasi-steady Lagrangian transport patterns from the ocean circulation: An application to the Gulf of Mexico. *Scientific Reports*, 8(1), 5218. <https://doi.org/10.1038/s41598-018-23121-y>.
- Fairall, C. W., Bradley, E. F., Hare, J. E., Grachev, A. A., & Edson, J. B. (2003). Bulk parameterization of air-sea fluxes: Updates and verification for the COARE algorithm. *Journal of Climate*, 16(4), 571–591.
- Fayman, P., Ostrovskii, A., et al. (2019). Submesoscale eddies in Peter the Great Bay of the Japan/East Sea in winter. *Ocean Dynamics*, 69(4), 443–462. <https://doi.org/10.1007/s10236-019-01252-8>.
- Fayman, P., Prants, S., Budyansky, M., & Uleysky, M. Y. (2019). Coastal summer eddies in the Peter the Great Bay of the Japan sea: In situ data, numerical modeling and Lagrangian analysis. *Continental Shelf Research*, 181, 143–155. <https://doi.org/10.1016/j.csr.2019.05.002>.
- Fifani, G., Baudena, A., et al. (2021). Drifting speed of Lagrangian fronts and oil spill dispersal at the ocean surface. *Remote Sensing*, 13(22), 4499. <https://doi.org/10.3390/rs13224499>.
- Flather, R. (1976) A tidal model of the north-west European continental shelf. In *Continental Shelf Dynamics: Seventh Liège Colloquium on Ocean Hydrodynamics*, vol. 10 of *Mémoires de la Société royale des sciences de Liège*, ser. 6, 141–164 (Siège de la Société, Université, Liège.)
- García-Sánchez, G., Mancho, A., & Wiggins, S. (2022). A bridge between invariant dynamical structures and uncertainty quantification. *Communications in Nonlinear Science and Numerical Simulation*, 104, 106016. <https://doi.org/10.1016/j.cnsns.2021.106016>.
- Good, S., Fiedler, E., et al. (2020). The current configuration of the OSTIA system for operational production of foundation sea surface temperature and ice concentration analyses. *Remote Sensing*, 12(4), 720. <https://doi.org/10.3390/rs12040720>.
- Guo, W., & Wang, Y. (2009). A numerical oil spill model based on a hybrid method. *Marine Pollution Bulletin*, 58(5), 726–734. <https://doi.org/10.1016/j.marpolbul.2008.12.015>.

- Haller, G. (2002). Lagrangian coherent structures from approximate velocity data. *Physics of Fluids*, 14(6), 1851–1861. <https://doi.org/10.1063/1.1477449>.
- Harrison, C. S., & Glatzmaier, G. A. (2012). Lagrangian coherent structures in the California Current System—sensitivities and limitations. *Geophysical & Astrophysical Fluid Dynamics*, 106(1), 22–44. <https://doi.org/10.1080/03091929.2010.532793>.
- Hernández-Carrasco, I., López, C., Hernández-García, E., & Turiel, A. (2011). How reliable are finite-size Lyapunov exponents for the assessment of ocean dynamics? *Ocean Modelling*, 36(3–4), 208–218. <https://doi.org/10.1016/j.ocemod.2010.12.006>.
- Isobe, A., & Isoda, Y. (1997). Circulation in the Japan Basin, the Northern Part of the Japan Sea. *Journal of Oceanography*, 53(4), 373–381.
- Keating, S. R., Smith, K. S., & Kramer, P. R. (2011). Diagnosing lateral mixing in the upper ocean with virtual tracers: Spatial and temporal resolution dependence. *Journal of Physical Oceanography*, 41(8), 1512–1534. <https://doi.org/10.1175/2011JPO4580.1>.
- Keramea, P., Spanoudaki, K., Zodiatis, G., Gikas, G., & Sylaios, G. (2021). Oil spill modeling: A critical review on current trends, perspectives, and challenges. *Journal of Marine Science and Engineering*, 9(2), 181. <https://doi.org/10.3390/jmse9020181>.
- Korotenko, K. A., Dietrich, D. E., & Bowman, M. J. (2003). Modeling of the circulation and transport of oil spills in the Black Sea. *Oceanology*, 43(4), 474–484.
- Korotenko, K., Mamedov, R., Kontar, A., & Korotenko, L. (2004). Particle tracking method in the approach for prediction of oil slick transport in the sea: Modelling oil pollution resulting from river input. *Journal of Marine Systems*, 48(1–4), 159–170. <https://doi.org/10.1016/j.jmarsys.2003.11.023>.
- Ladychenko, S. Y., & Lobanov, V. B. (2013). Mesoscale eddies in the area of Peter the Great Bay according to satellite data. *Izvestiya, Atmospheric and Oceanic Physics*, 49(9), 939–951. <https://doi.org/10.1134/s0001433813090193>.
- Lin, S. (1997). A finite-volume integration method for computing pressure gradient force in general vertical coordinates. *Quarterly Journal of the Royal Meteorological Society*, 123(542), 1749–1762. <https://doi.org/10.1002/qj.49712354214>.
- MacFadyen, A., Watabayashi, G. Y., Barker, C. H. & Beegle-Krause, C. J. (2011). *Tactical modeling of surface oil transport during the Deepwater Horizon spill response*. In Liu, Y., MacFadyen, A., Ji, Z.-G. & Weisberg, R. H. (eds.) *Monitoring and Modeling the Deepwater Horizon Oil Spill: A Record Breaking Enterprise*, vol. 195 of Geophysical Monograph Series, 167–178 (American Geophysical Union (AGU), Washington, D.C.). <https://doi.org/10.1029/2011GM001128>
- Michel, J. & Fingas, M. (2016). *Oil spills: Causes, consequences, prevention, and countermeasures*. In Crawley, G. M. (ed.) *Fossil Fuels*, vol. 1 of World Scientific Series in Current Energy Issues, chap. 7, 159–201 (World Scientific, Singapore). https://doi.org/10.1142/9789814699983_0007
- Miyazawa, Y., Zhang, R., et al. (2009). Water mass variability in the western North Pacific detected in a 15-year eddy resolving ocean reanalysis. *Journal of Oceanography*, 65(6), 737–756. <https://doi.org/10.1007/s10872-009-0063-3>.
- Ohshima, K. I., & Simizu, D. (2008). Particle tracking experiments on a model of the Okhotsk Sea: Toward oil spill simulation. *Journal of Oceanography*, 64(1), 103–114. <https://doi.org/10.1007/s10872-008-0008-2>.
- Olascoaga, M. J., & Haller, G. (2012). Forecasting sudden changes in environmental pollution patterns. *Proceedings of the National Academy of Sciences*, 109(13), 4738–4743. <https://doi.org/10.1073/pnas.1118574109>.
- Ono, J., Ohshima, K. I., et al. (2013). Particle-tracking simulation for the drift/diffusion of spilled oils in the Sea of Okhotsk with a three-dimensional, high-resolution model. *Journal of Oceanography*, 69(4), 413–428. <https://doi.org/10.1007/s10872-013-0182-8>.
- Pan, Q., Yu, H., et al. (2020). Fate and behavior of Sanchi oil spill transported by the Kuroshio during January–February 2018. *Marine Pollution Bulletin*, 152, 110917. <https://doi.org/10.1016/j.marpolbul.2020.110917>.
- Pierrehumbert, R. T. (1991). Chaotic mixing of tracer and vorticity by modulated travelling Rossby waves. *Geophysical & Astrophysical Fluid Dynamics*, 58(1–4), 285–319. <https://doi.org/10.1080/03091929108227343>.
- Prants, S. V., Uleysky, M. Y. & Budyansky, M. V. (2017). Lagrangian Oceanography: Large-scale Transport and Mixing in the Ocean. *Physics of Earth and Space Environments (Springer)*. <https://doi.org/10.1007/978-3-319-53022-2>
- Prants, S. V. (2014). Chaotic Lagrangian transport and mixing in the ocean. *The European Physical Journal Special Topics*, 223(13), 2723–2743. <https://doi.org/10.1140/epjst/e2014-02288-5>.
- Prants, S. (2022). Marine life at Lagrangian fronts. *Progress in Oceanography*, 204, 102790. <https://doi.org/10.1016/j.poccean.2022.102790>.
- Prants, S. V., Budyansky, M. V., Ponomarev, V. I., & Uleysky, M. Y. (2011). Lagrangian study of transport and mixing in a mesoscale eddy street. *Ocean Modelling*, 38(1–2), 114–125. <https://doi.org/10.1016/j.ocemod.2011.02.008>.
- Prants, S. V., Budyansky, M. V., & Uleysky, M. Y. (2014). Lagrangian fronts in the ocean. *Izvestiya, Atmospheric and Oceanic Physics*, 50(3), 284–291. <https://doi.org/10.1134/s0001433814030116>.
- Prants, S. V., Budyansky, M. V., & Uleysky, M. Y. (2014). Lagrangian study of surface transport in the Kuroshio Extension area based on simulation of propagation of Fukushima-derived radionuclides. *Nonlinear Processes in Geophysics*, 21(1), 279–289. <https://doi.org/10.5194/npg-21-279-2014>.
- Prants, S. V., Andreev, A. G., Budyansky, M. V., & Uleysky, M. Y. (2015). Impact of the Alaskan Stream flow on surface water dynamics, temperature, ice extent, plankton biomass, and walleye pollock stocks in the eastern Okhotsk Sea. *Journal of Marine Systems*, 151, 47–56. <https://doi.org/10.1016/j.jmarsys.2015.07.001>.
- Prants, S. V., Fayman, P. A., Budyansky, M. V., & Uleysky, M. Y. (2022). Simulation of winter deep slope convection in Peter the Great Bay (Japan Sea). *Fluids*, 7(4), 134. <https://doi.org/10.3390/fluids7040134>.
- Qiao, F., Wang, G., et al. (2019). Modelling oil trajectories and potentially contaminated areas from the Sanchi oil spill. *Science of The Total Environment*, 685, 856–866. <https://doi.org/10.1016/j.scitotenv.2019.06.255>.
- Shadden, S. C., Lekien, F., & Marsden, J. E. (2005). Definition and properties of Lagrangian coherent structures from finite-time Lyapunov exponents in two-dimensional aperiodic flows. *Physica D: Nonlinear Phenomena*, 212(3–4), 271–304. <https://doi.org/10.1016/j.physd.2005.10.007>.

- Shchepetkin, A. F., & McWilliams, J. C. (2005). The regional oceanic modeling system (ROMS): A split-explicit, free-surface, topography-following-coordinate oceanic model. *Ocean Modelling*, 9(4), 347–404. <https://doi.org/10.1016/j.ocemod.2004.08.002>.
- Shevchenko, G. V., Gorbunov, A. O., & Korolev, P. Y. (2017). Hydrodynamic and geomorphological conditions in the construction area of the «Port «Vera» (Ussuri Bay). *Fundamentalnaya i Prikladnaya Gidrofizika*, 10(2), 49–62 (**[in Russian]**).
- Takematsu, M., Nagano, Z., Ostrovski, A. G., Kim, K., & Volkov, Y. (1999). Direct measurements of deep currents in the Northern Japan Sea. *Journal of Oceanography*, 55(2), 207–216. <https://doi.org/10.1023/a:1007842013257>.
- Tian, W., Yu, M., Wang, G., & Guo, C. (1999). Pollution trend in the Tumen River and its influence on regional development. *Chinese Geographical Science*, 9(2), 146–150. <https://doi.org/10.1007/bf02791365>.
- Umlauf, L., & Burchard, H. (2003). A generic length-scale equation for geophysical turbulence models. *Journal of Marine Research*, 61(2), 235–265. <https://doi.org/10.1357/002224003322005087>.
- Varlamov, S. M., & Yoon, J.-H. (2003). Operational simulation of oil spill in the Sea of Japan. *Reports of Research Institute for Applied Mechanics, Kyushu University*, 51, 15–20.
- Varlamov, S. M., Yoon, J.-H., Hirose, N., Kawamura, H., & Shiohara, K. (1999). Simulation of the oil spill processes in the Sea of Japan with regional ocean circulation model. *Journal of Marine Science and Technology*, 4(3), 94–107. <https://doi.org/10.1007/s007730050012>.
- Yurasov, G. I., & Yarichin, V. G. (1991). *The water currents in the sea of Japan*. Vladivostok: FEB AS USSR (**[in Russian]**).
- Zweng, M., & Reagan, J. et al. (2019). *World Ocean Atlas 2018*, Volume 2: Salinity. A. Mishonov, Technical Editor, NOAA Atlas NESDIS 82, 50 pp.

(Received August 5, 2022, revised November 23, 2022, accepted November 23, 2022, Published online January 9, 2023)